PROC. 21st INTERNATIONAL CONFERENCE ON MICROELECTRONICS (MIEL'97), VOL.2, NIŠ, YUGOSLAVIA, 14-17 SEPTEMBER, 1997

Technology CAD: Process and Device Simulation

H. Kosina and S. Selberherr

Abstract—**The state of the art in self-consistent numerical modeling of semiconductor devices and their fabrication processes is reviewed. Particular emphasis is put on the models for dopant profile formation, namely ion-implantation and annealing, and on models for carrier transport.**

I. Introduction

Continuous advances over the past years in integrated circuit technology impose new challenges on modeling of fabrication processes and electrical behavior of semiconductor devices. The routine utilization of process and device simulation has become indispensable for the development and redesign of ULSI devices as well as for power devices.

During fabrication of a modern integrated circuit numerous process steps, which exploit a broad variety of physical and chemical effects, are applied one after the other onto the semiconductor wafer. Nowadays for virtually all these process steps one or more, usually very specialized, simulation tools are available. These tools deal with the simulation of optical lithography comprising the simulation of the areal image, exposure of the photoresist, and resist development. Furthermore, topography simulation is applied to etching and deposition processes, which change the shape of the wafer surface. Very accurate simulation tools are required for ion-implantation used to selectively dope semiconductors as well as for high temperature processes such as dopant diffusion and oxidation of silicon. Especially for the high temperature processes not only is simulation used to give input data for device simulation, but also to understand the effect of successive process steps on doping distribution and wafer topography.

A brief review on the state of the art in modeling the processes listed above is given, and some more emphasis is put on the processes for dopant profile formation, which are mainly ion-implantation and annealing giving rise to, in case of shallow junction formation unwanted, dopant diffusion.

While the coöperation of a variety of process simulation tools generates a model of the desired semiconductor structure a device simulation tool computes the electrical characteristics of the resulting electronic device. Device simulation based on the self-consistent solution of the basic semiconductor equations dates back to the famous work of Gummel in 1964 [1]. Since then numerical device modeling has been applied to nearly all important devices. The current relations responsible for modeling carrier transport through a device have been frequently subject of discussions, in particular in view of their applicability to submicron devices. We present transient simulations based on the drift-diffusion transport model and discuss in more detail the hydrodynamic transport model.

II. Lithography Simulation

Decreasing dimensions and increasing non-planarity of semiconductor devices makes the optical lithography process a very critical one in semiconductor manufacturing. Simulation has to be capable of assessing phenomena such as light scattering from wafer topography or defraction through photomask apertures. Rigorous numerical models of wave propagation are needed because typical feature sizes are on the order of a wavelength. In this regime, neither the Rayleigh approximation nor geometric optics suffices. The solution of the Maxwell equations by means of the time-domain finite-difference method can be very time-consuming [2], whereas the waveguide method, a spatial frequency-domain method for solving the Maxwell equations, appears to be more efficient [3][4]. As boundary condition the light intensity incidenting on top of the wafer, also referred to as areal image, has to be known. This can be obtained by another simulation taking into account light propagation through the optical system and the light transmission through the photomask [5]. Once the light propagation within the optically nonlinear resist is known, the chemical reaction of the photosensitive compound is computed, and the latent bulk image is obtained. Development of the photoresist is treated as an isotropic etch process, with etch rates being determined by the previously calculated bulk image.

III. Topography Simulation

Topography simulation assists in understanding the time evolution of topographical features in advanced semiconductor structures. The numerical methods and algorithms applied to the movement of the actual surface play a key role because they determine accuracy, robustness and efficiency of a simulation tool.

Many algorithms also applicable to topography simulation have been reported for photoresist development in lithography simulation [6][7][8][9][10][11], and fewer methods have been proposed for the simulation of etching and deposition processes [12][13][14][15]. Basically, there are two types of algorithms feasible for multi-dimensional topography simulation. The first type of algorithms represent the surface of the material being etched by a mesh of triangular facets [12]. Either the mesh points or the facets are moved according to the lo-

0-7803-3664-X/97/$10.00 © 1997 IEEE

cal etch rates. In general, these algorithms yield highly accurate results, though with potential topological instabilities such as erroneous surface loops which result from a growing or shrinking surface intersecting with itself. In three dimensions, the detection of such surface loops takes a large algorithmic overhead.

Volume removal methods are the second type of methods. The material being etched is divided into a large array of rectangular prismatic cells, each of which is characterized as etched, unetched, or partially etched. During etching cells are removed one by one according to the local etch rate and the number of cell faces exposed to the etching medium. Volume removal methods have the potential to handle arbitrary geometries [7][8][9], but unfortunately they suffer from inherent inaccuracy as they favor certain mesh-dependent directions.

A more general approach to surface evolution is presented in [16]. Fundamental morphological operations originally employed in digital image processing are performed on a cellular material representation. The latter fact also enables efficient shadow and visibility computation which are needed to determine the particle flux of directly and indirectly incident particles. Such simulations allow to investigate step coverage effects (see Fig. 1).

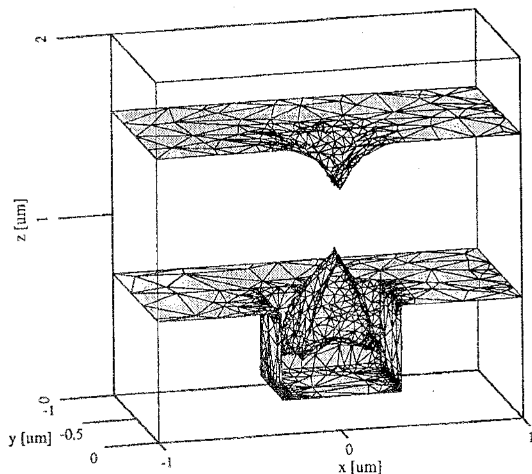

Fig. 1. Simulation of a sputter deposition.

Topography simulation allows on one hand a better physical understanding of the applied etching and deposition processes, and on the other hand it provides the geometry information needed for subsequent process and device simulation.

IV. Ion Implantation

Ion implantation is the method of choice to selectively introduce dopants into the layers of an integrated circuit [17]. One of the first atomistic approaches to estimate implantation profiles was performed by Lindhard, Scharff and Schiøtt (LSS theory) [18]. Under the assumption of Gaussian profiles, the mean projected range and the standard deviation of the implantation profile are calculated. Tabulated values of these so-called LSS parameters can be found, for instance, in [19]. Since then elaborate analytical methods have been developed to describe dopant distributions. For the analytical description of implantation profiles it is assumed that they can be closely approximated by statistical functions. Suitable distributions are the so-called Pearson distributions. They are derived as solutions $f(x)$ of the differential equation

$$\frac{\mathrm{d}f(y)}{\mathrm{d}y} = \frac{y-a}{b_0 + b_1 y + b_2 y^2} f(y)\,, \qquad y = x - R_p. \qquad (1)$$

The parameters a, b_0, b_1, and b_2 can be expressed in terms of the moments of the distribution, namely standard deviation σ_p, skewness γ_1, and kurtosis β_2. R_p denotes the mean projected range. Depending on the roots of the denominator polynomial of (1) seven types of solutions are distinguished.

It should be noted that the Perason distributions themselves have no direct meaning for ion implantation. The justification of applying them to ion implantation profiles is given by the fact that they resemble nearly all ion implantation profiles very closely, and that closed formulas exist for them. In a few cases the Pearson distributions do not agree well with measured profiles, they have to be adapted by adding exponential tails [20] or by doing other manipulations. These manipulations appear justified since the only goal of using analytical functions is to fit measurements.

Ion implantation profiles are characterized by the moments as a function of implantation energy and dose [21]. In the regime of low and very high doses it is sufficient to assume that the shape of the implantation profiles is a function of the implantation energy. The dose is then used only as a multiplicative factor. For the intermediate doses close to the amorphization dose, this simple assumption does not suffice, and recent trends go either in the direction of tabulating the distribution moments as a function of dose and energy [21][22] or to add two Pearson profiles, one for the amorphous part and one for the crystalline part of the profile [23].

If the ions are implanted through passivating or scattering layers two analytical profiles have to be added by some empirical method, for instance, by the so-called NRS-algorithm (Numerical Range Scaling) [24].

Two-dimensional analytical dopant profiles are obtained from the one-dimensional dopant profiles by performing a convolution with a lateral Gaussian distribution [25]. In [26] a further improvement by using convolutions with symmetrical Pearson functions and depth dependent moments has been proposed.

In most process simulators such analytical models of ion-implanted profiles are incorporated because they allow a quick calculation of the results, however, at the expense of reduced accuracy in realistic structures such as multilayer structures or trenches.

Compared to the analytical methods based on distribution functions the Monte Carlo technique allows to model ion-implantation more accurately. The trajectory of a single ion is traced on its way through the solid until it comes to rest. On its way, the ion collides with other atoms, transfers energy to these atoms, or is slowed down by interaction with the electron shells of the target atoms. The energy passed to other atoms can be high enough such that these atoms are displaced from their lattice position and may interact with other atoms. By simulating a large number of trajectories, the final distribution of atoms in the target material can be determined.

When energetic ions move nearly parallel to a major axis or plane in a crystal, they may be steered down the open channels between the rows or planes of atoms. This so-called channeling effect [27] leads to increased ion ranges for part of the implanted ions. In Monte Carlo simulation channeling is accounted for by including proper models for the electronic stopping power [28][29]. Implantation damage, i.e. the gradual destruction of the crystalline target by the implanted ions, is described by damage accumulation models [29][30]. In miniaturized structures three-dimensional effects are gaining importance, an implementation of the Monte Carlo technique combining both the latest physical models and the ability to deal with complex three-dimensional structures are reported in [31][32]. Fig. 2 shows a three-dimensional simulation after [32].

An approach of similar rigor is given by the solution of the Boltzmann transport equation, which describes the motion of the dopants in the phase space. This method relies on the same scattering principles as the Monte Carlo technique. However, changes in the composition of the target material are not easily included. As a continuum method, it gives smoother dopant profiles in less time [33][34].

Drawbacks of both the Monte Carlo and the Boltzmann solution technique are the high computation times, which even increases considerably if crystalline targets are considered instead of amorphous ones. This is the reason why the simpler analytical methods found wide spread application in process simulation tools. These tools have to be capable of performing repeated calculations for the purpose of technology optimization in affordable time.

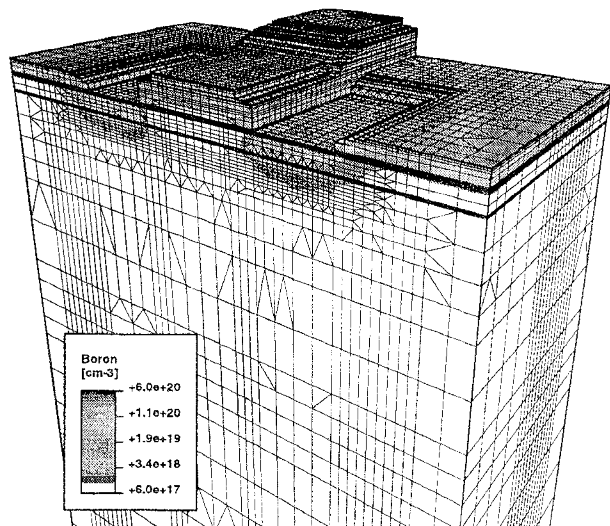

Fig. 2. Boron concentration in 0.5 μm gate length p-MOS transistor simulated with the Monte Carlo method. The p^+ source/drain implantation was performed at 45 keV and a dose of $5 \cdot 10^{15}$ cm^{-2}.

V. Diffusion

During process steps at elevated temperatures, dopant atoms migrate due to statistical motions. The main assumptions made when modeling dopant diffusion are first that electrically active dopant atoms reside on substitutional sites of the lattice, and second, that dopant atoms can diffuse only due to the assistance of diffusion vehicles. As diffusion vehicles one usually considers vacancies and silicon self-interstitials in various charge states. A review on this subject is given by Fahey et al. [35].

The simplest case, the so-called intrinsic case, is when the dopant atoms are very diluted in a perfect crystal and if no chemical reaction takes place at the surface of the semiconductor. In this case, the diffusion vehicles are assumed not to be influenced by the dopants and to have a constant concentration with respect to time and position. This allows to get rid of the diffusion vehicles in the diffusion model, and to describe the redistribution of dopants by the two laws of Fick [36]. If the dopant concentration exceeds the intrinsic carrier concentration an electric field will be present in the wafer. This field acts on all charged point defects, namely intrinsic point defects, ionized dopants, and charged dopant-point defect pairs. In the first estimations of this effect the field effect on the diffusion vehicles have been neglected, and the field effect on the diffusion has been described by modifying the flux equation to [37]

$$\vec{J} = -D_i \cdot \nabla C + z \cdot \mu_i \cdot C \cdot \nabla \varphi \quad (2)$$

At the surface the boundary condition $\vec{J} \cdot \vec{n} = 0$ applies. In (2), $\vec{J}$ and C denote the flux and the concentration of the dopant atoms, respectively, φ describes the electrostatic potential and z the charge state of the dopant ($z = 1$ for singly charged acceptors, and $z = -1$ for

singly charged donors). The diffusion coefficient D_i is only a function of temperature, and usually it follows an Arrhenius law. The mobility μ_i is related to the diffusion coefficient D_i by the Einstein relation, and the electrostatic potential can be computed from Poisson's equation. The electron and hole concentrations can be obtained by assuming Boltzmann statistics. The error caused by this simplification is sufficiently small [38].

The effect of the electric field can be estimated by assuming charge neutrality in the form $n - p + \sum z_i \cdot C_i = 0$, where the C_i are the concentration of different dopant species. This assumption allows to calculate the electrostatic potential explicitly and again with low errors if the impurity diffusion length is several times the Debye length [39]. The flux equation for dopant j is then given by

$$\vec{J}_j = -D_{jj} \cdot \left(1 + \frac{C_j}{\sqrt{4 \cdot n_i^2 + (\sum z_i \cdot C_i)^2}}\right) \cdot \nabla C_j - \frac{D_{ij} \cdot z_j \cdot C_j}{\sqrt{4 \cdot n_i^2 + (\sum z_i \cdot C_i)^2}} \sum_{i \neq j} z_i \cdot \nabla C_i. \qquad (3)$$

From this equation it can be seen that the diffusion coefficient for the dopant j increases by a factor which has a value close to one for concentrations below the intrinsic concentrations and a maximum value of two for high concentrations. Furthermore, if more than one dopant is present the diffusion of the dopants will be coupled due to the electric field (Fig. 3).

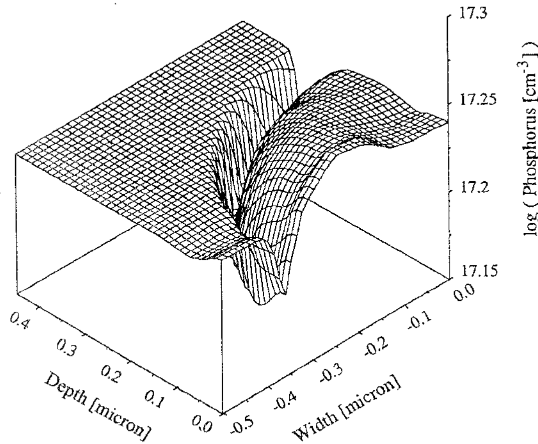

Fig. 3. Source area of a 0.35 μm p-channel MOS transistor: the originally constant substrate (phosphorus) doping has become lower in the vicinity of the pn-junction due to the field coupling to the source (boron) profile.

It has bee found out, however, that the field enhancement predicted by (3) is not sufficient to explain measured data. To this point the analysis did not include the diffusion vehicles, and it is in a strict sense valid only if all diffusion vehicles are assumed to be neutral.

The additional diffusion enhancement observed experimentally has then be attributed to vacancies as diffusion vehicles in various charge states. The diffusion via vacancies in each charge state is proportional to the concentration of the respective vacancy species. By applying a simple mass action law one obtains for the concentration of the singly and doubly negative charged vacancies ($C_{V^-}, C_{V^=}$) normalized by their intrinsic values ($C_{V^-}^i, C_{V^=}^i$) [40]

$$\frac{C_{V^-}}{C_{V^-}^i} = \frac{n}{n_i}, \qquad \frac{C_{V^=}}{C_{V^=}^i} = \left(\frac{n}{n_i}\right)^2. \qquad (4)$$

The diffusion coefficients for, e.g. donors, can then be written in the form

$$D = D_i^0 + D_i^- \cdot \frac{n}{n_i} + D_i^= \cdot \left(\frac{n}{n_i}\right)^2 \qquad (5)$$

where the parameters D_i^0, D_i^- and $D_i^=$ characterize the contributions of the neutral, singly and doubly charged vacancies to the diffusion coefficient. The diffusion coefficient for intrinsic concentrations is obtained as $D_i = D_i^0 + D_i^- + D_i^=$. Under the assumption of vacancies in various charge states as diffusion vehicles the influence of their gradients on the diffusion cannot be neglected. Nevertheless, the model has great success up to now and the most popular diffusion coefficients and nonlinearity coefficients have been proposed by Fair [40].

If the dopant concentration becomes so high that the solubility limit in silicon is approached, the dopants will form precipitates or clusters. Precipitates may contain many thousands of dopant atoms and are considered as regions of the crystal that have formed a second phase. In contrast, clusters are composed of a few dopant atoms in specific configurations, and are ionized at diffusion temperatures. Clustered dopants are assumed not to diffuse and to be electrically inactive at room temperature. A popular clustering model for arsenic can be found in [41]. Fig. 4 shows a boron profile part of a p-MOS transistor simulated with a static clustering model [42].

All of the above mentioned influences on the diffusion coefficient share the assumption that the diffusion coefficient is a local function of the electric field and of the concentration of all involved dopants. Unfortunately, this cannot be generally assumed. If the high temperature treatment goes with an oxidation of the wafer, the diffusion, for instance of boron and phosphorus, is enhanced appreciably (OED – Oxidation Enhanced Diffusion) [43], whereas the diffusion of antimony is retarded (ORD – Oxidation Retarded Diffusion). The effect on the diffusion coefficient depends on the crystal orientation as well as on the dopant concentration [44]. This suggests some long range influence from the surface which is again attributed to the diffusion vehicles.

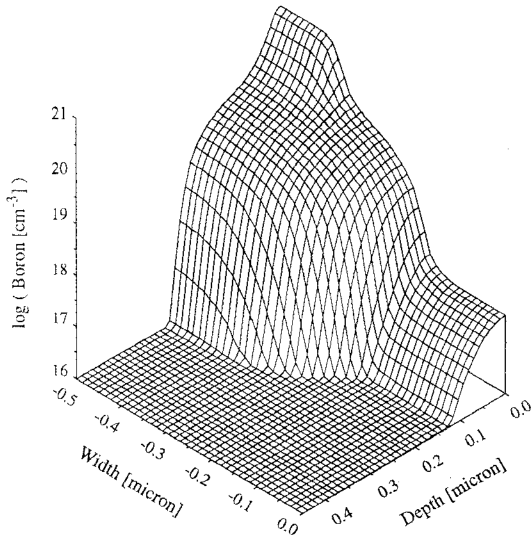

Fig. 4. Source doping profile of a 0.35 μm p-channel MOS transistor. The narrow peak on top of the diffused boron profile comprises immobile clusters of boron atoms.

In most theories it is assumed that during oxidation of silicon interstitials are emitted at the oxidizing surface.

Under oxidizing conditions, the concentration of silicon self-interstitials is enhanced and that of vacancies is decreased. In an attempt do include the point defect concentrations the intrinsic diffusion coefficient is usually split into a vacancy and an interstitial contribution of the form

$$D = D_i \cdot \left(f_I \cdot \frac{C_I}{C_I^*} + (1 - f_I) \cdot \frac{C_V}{C_V^*} \right) \tag{6}$$

with the diffusion coefficient under inert and intrinsic conditions D_i, and the interstitial and vacancy concentrations C_I and C_V, respectively. The asterisks denote thermodynamic equilibrium conditions. The factor f_I characterizes the contribution of the interstitials to the diffusion coefficient. It takes the value one if the diffusion goes exclusively via interstitials and zero if it goes exclusively via vacancies.

To complete the model additional diffusion equations for the point defects have to be solved:

$$\frac{\partial C_I}{\partial t} = \nabla(D_I \cdot \nabla C_I) - k_f \cdot (C_I \cdot C_V - C_I^* \cdot C_V^*) \, , \tag{7}$$

$$\frac{\partial C_V}{\partial t} = \nabla(D_V \cdot \nabla C_V) - k_f \cdot (C_I \cdot C_V - C_I^* \cdot C_V^*) \, . \tag{8}$$

The symbols D_I, D_V, and k_f denote the diffusion coefficients for interstitials and vacancies, and the bulk recombination constant, respectively.

The reported values for the diffusion coefficients and the equilibrium concentrations cover a range of several orders of magnitude, and very little is known about the bulk recombination constant. The reason for this might be that various combinations of parameters, which cannot be determined individually, give dopant profiles of nearly the same shape.

As boundary conditions at the oxidizing surface one commonly assumes surface recombination for interstitials and vacancies, as well as interstitial generation.

$$\begin{aligned} \vec{J_I} \cdot \vec{n} &= k_I \cdot (C_I - C_I^*) - C_{Si} \cdot \Theta \cdot \frac{\mathrm{d}X_o}{\mathrm{d}t} \\ \vec{J_V} \cdot \vec{n} &= k_V \cdot (C_V - C_V^*) \end{aligned} \tag{9}$$

The parameters k_I and k_V are the surface recombination velocities for interstitials and vacancies, respectively, C_{Si} denotes the density of lattice sites of silicon, Θ the fraction of silicon atoms that is not oxidized, and $\mathrm{d}X_o/\mathrm{d}t$ represents the oxide growth rate.

Whereas boron profiles can be well modeled by including the effects described so far, the diffusion of high phosphorus concentrations cannot be described as easily. The recent approaches to phosphorus diffusion are based on multistream diffusion [45][46]. For these models it is assumed that phosphorus diffuses via dopant-point defect pairs (PI, PV). The formation of these pairs from interstitials I and vacancies V can be described by

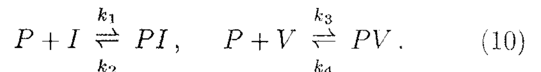

$$P + I \underset{k_2}{\overset{k_1}{\rightleftharpoons}} PI \, , \qquad P + V \underset{k_4}{\overset{k_3}{\rightleftharpoons}} PV \, . \tag{10}$$

The parameters k_1 to k_4 denote rate constants. If different charge states of interstitials, vacancies and the complexes are included, one ends up in quite a number of coupled nonlinear partial differential equations for which it is not feasible to determine all the involved parameters. Therefore, it is crucial for practical simulation to eliminate second order influences where possible, for instance by assuming local thermal equilibrium for point defect-dopant pair formation reaction. The remaining parameters are fitted to experiments, however, it is often possible to reproduce a certain result by different sets of parameters. This gives rise to a wide spread in the parameter values reported in the literature.

Process simulation tools must be able to deal with dopant diffusion in three-dimensional structures in order to be applicable to highly down-scaled processes. Thus much effort has been expended in finding solutions for related problems such as geometry definition, grid generation and grid refinement, discretization, linear solvers, and visualization [47].

Because the electrical behavior of a semiconductor device strongly depends on the dopant profile an accurately modeled dopant profile is a crucial prerequisite for the subsequent device simulation.

VI. Device Simulation

The vast majority of todays routinely performed device simulations are based on a numerical solution of

the basic semiconductor equations which include drift-diffusion current relations [48]. The efficiency of this numerical device model allows its extensive use in device optimization.

A device of a modern ULSI circuit is characterized by large electric fields in conjunction with steep gradients of the electric field and of the carrier concentrations. Under these conditions, the accuracy of the widely used drift-diffusion model becomes questionable. More sophisticated device models, such as the hydrodynamic and energy-transport models ([49][50][51][52][53][54][55]), the spherical harmonics expansion method ([56][57]) and the Monte Carlo technique ([58][59][60]), overcome these limitations. However, the increased physical rigor of a model comes at the expense of increased computation times. This fact prevented wide spread application of the models in the past, and probably in the near future.

A. *Numerical Aspects*

In this section we describe some of the numerical methods used in the recently developed device simulator MINIMOS-NT [61].

To handle handle complex device structures it is useful to partition the geometry in independent regions, so-called segments. Specific to each segment are the material type, the set of models and parameters, and even the set of partial differential equations. If boundary conditions are generally definedable, it is possible to connect segments via passive circuit elements. Interface conditions link segments together and make it possible to consider hetero-interfaces with abrupt changes of band-edge energies and other material properties. The partitioning of the simulation domain into different segments allows to specify volume models inside the segments and interface models at their boundaries in an independent manner.

It is well known that numerical solution methods for the hydrodynamic transport model suffers from moderate convergence behavior and the propensity for instability. This situation can be improved by a block-iterative scheme. Iteration is performed over two blocks, one comprising Poisson's and the carrier continuity equations, and one comprising the carrier continuity and energy balance equations. It should be noted that the carrier continuity equations are solved in both blocks, which means that some redundancy has been introduced. However, convergence and stability are considerably improved. The final accuracy is then obtained by a few full Newton cycles.

When solving the transient semiconductor equations [48] in a decoupled manner, stability problems arise with Poisson's equation. Following the reasoning of Mock [62], stability independent of the time step can be achieved by employing instead of the original Poisson equation its time derivative. The Poisson equation differentiated with respect to time states continuity of the total current within the segments.

As an example an n-channel charge-coupled device (CCD) consisting of 15 gates has been simulated in two space dimension. Until now, transient simulation has not been practicable because of the high requirements of computational resources, hence only single CCD cells have been simulated [63][64]. The structure of the simulated three-phase clock CCD is depicted in Figure 5. Figure 6 shows the charge that has passed through the source, drain and bulk contacts, respectively.

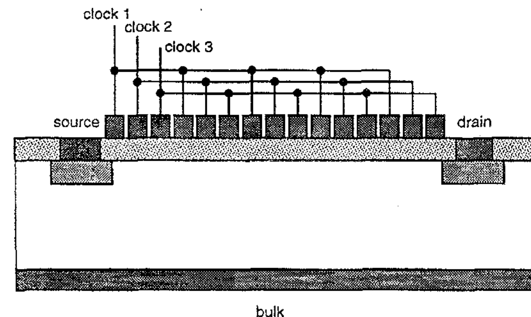

Fig. 5. Structure of the CCD. The source and drain contacts were held constant at $U_S = U_D = 0V$, the bulk contact at $U_B = -1V$. The voltages applied to the gates varied between $U_G = -1V$ and $U_G = 5V$.

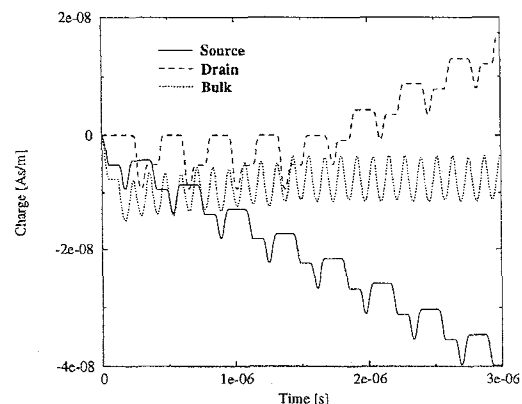

Fig. 6. Charge passed through the contacts of a 15 gate CCD

B. *Hydrodynamic Simulation*

The hydrodynamic approach extends beyond the drift-diffusion approach by allowing the carrier temperatures to differ from the lattice temperature. Coefficients to be modeled properly such as mobilities and ionization coefficients can now be functions of some higher order moments [65][66].

In the following we summarize the generalized equations of the hydrodynamic model with extensions for non-uniform band-edge energies and non-uniform effective density of states. These parameters become

position-dependent, for example, in semiconductor alloys with spatially changing mole fraction, or in heavily doped regions where band-gap narrowing occurs. In the hydrodynamic model the current relations are of the form:

$$\vec{J}_n = q \cdot \mu_n \cdot n \cdot \left(\nabla \left(\frac{E_C}{q} - \psi \right) + \frac{k_B}{q} \cdot \frac{N_C}{n} \cdot \nabla \left(\frac{n \cdot T_n}{N_C} \right) \right) \quad (11)$$

$$\vec{J}_p = q \cdot \mu_p \cdot p \cdot \left(\nabla \left(\frac{E_V}{q} - \psi \right) - \frac{k_B}{q} \cdot \frac{N_V}{p} \cdot \nabla \left(\frac{p \cdot T_p}{N_V} \right) \right) \quad (12)$$

Here, E_C and E_V denote the band-edge energies, N_C and N_V the effective density of states of the respective bands. Spatial variation of the mole fraction of semiconductor alloys results in non-uniform parameters $E_{C,V}$ and $N_{C,V}$, an effect properly treated by equations (11) and (12).

The following equations, also called energy balance equations, state continuity of the energy fluxes $\vec{S}_n$ and $\vec{S}_p$, for both electrons and holes.

$$\frac{\partial(n \cdot w_n)}{\partial t} + \nabla \vec{S}_n = \nabla \left(\frac{E_C}{q} - \psi \right) \cdot \vec{J}_n - R \cdot w_n - n \cdot \frac{w_n - w_0}{\tau_{wn}} \quad (13)$$

$$\frac{\partial(p \cdot w_p)}{\partial t} + \nabla \vec{S}_p = \nabla \left(\frac{E_V}{q} - \psi \right) \cdot \vec{J}_p - R \cdot w_p - p \cdot \frac{w_p - w_0}{\tau_{wp}} \quad (14)$$

Here τ_{wn} and τ_{wp} are the respective energy relaxation times, and w_0 is the average energy in thermodynamic equilibrium. The average carrier energies w_n, w_p are related to the average velocities v_n, v_p and the hydrodynamic temperatures T_n, T_p by

$$w_n = \frac{1}{2} \cdot m_n^* \cdot v_n^2 + \frac{3}{2} \cdot k_B \cdot T_n \quad (15)$$

$$w_p = \frac{1}{2} \cdot m_p^* \cdot v_p^2 + \frac{3}{2} \cdot k_B \cdot T_p \quad (16)$$

The energy fluxes have the form

$$\vec{S}_n = \vec{Q}_n - (w_n + k_B \cdot T_n) \cdot \frac{\vec{J}_n}{q} \quad (17)$$

$$\vec{S}_p = \vec{Q}_p + (w_p + k_B \cdot T_p) \cdot \frac{\vec{J}_p}{q} \quad (18)$$

$\vec{Q}_n, \vec{Q}_p$ denote the carrier heat fluxes.

Discretization of the energy balance equations is not as straight forward as that of the carrier continuity equations. For this purpose several attempts to generalize the Scharfetter-Gummel scheme have been proposed [67][68]. In this work we follow the approach of Choi et al. [69], with extensions needed to handle spatially varying band-edge energies and effective density of states [70].

There are two mobility models commonly used in hydrodynamic simulations. Baccarani and Wordeman [51] assume that the diffusion coefficient can well be approximated by a constant. The Einstein relation, generalized to the non-equilibrium case, immediately yields

$$\mu_n = \mu_0 \cdot \frac{w_0}{w_n} \quad (19)$$

In [51] this expression has been combined with the empirical Caughey-Thomas relation for the field-dependent mobility. As result a weak temperature dependence of the energy relaxation time can be derived.

Hänsch et al. [71] propose an energy dependence for the mobility of the form

$$\mu_n = \frac{\mu_0}{1 + \alpha \cdot (w_n - w_0)} \quad (20)$$

$$\alpha = \frac{\mu_0}{(q \cdot \tau_{wn} \cdot v_{n,sat}^2)} \quad (21)$$

α contains parameters describing the asymptotic behavior for small and large electric fields. The energy relaxation time is assumed independent of any moment. Within this approach, a field-dependent mobility can be derived, which agrees very well with measured data in case of silicon.

The models (19) and (20) predict a behavior like $\mu \sim w^{-1}$ for high energies. For compound semiconductors, however, Monte Carlo calculations reveal severely different power laws, in the range between $\mu \sim w^{-2}$ and $\mu \sim w^{-5}$. A mobility model for this case has been proposed by Köpf et al.[72].

A well known characteristic of the method of moments is that the moment equation of order i always contains an $(i+1)$th order moment. In the case of the energy balance equation this next higher moment is of third order

$$\vec{Q}(\vec{r}) = \int \frac{m^*}{2} \cdot c(\vec{k})^2 \cdot \vec{c}(\vec{k}) \cdot f(\vec{k}, \vec{r}) \, d^3k \quad (22)$$

which has the physical meaning of a macroscopic heat flux density. Here $\vec{c}(\vec{k})$ denotes the random velocity defined as $\vec{c}(\vec{k}) = \vec{u}(\vec{k}) - <\vec{u}>$. In order to close the set of moment equations this higher order moment has to be related somehow to the lower order moments. For the heat flux one conventionally assumes Fourier's law

$$\vec{Q}(\vec{r}) = -\kappa(\vec{r}) \cdot \mathrm{grad}\, T(\vec{r}) \quad (23)$$

in conjunction with a generalized Wiedemann-Franz law

$$\kappa(\vec{r}) = \left(\frac{5}{2} + c' \right) \cdot \left(\frac{k_B}{q} \right)^2 \cdot \sigma(\vec{r}) \cdot T(\vec{r}) \quad (24)$$

for the thermal conductivity κ of the considered carrier gas.

In the following results of a hydrodynamic simulation of a high electron mobility transistor (HEMT) are

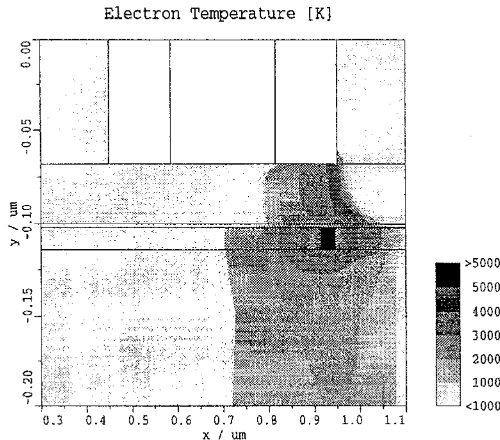

Fig. 7. Distribution of the electron temperature in a low-noise HEMT ($V_{DS} = 5V$, $V_{GS} = 1V$).

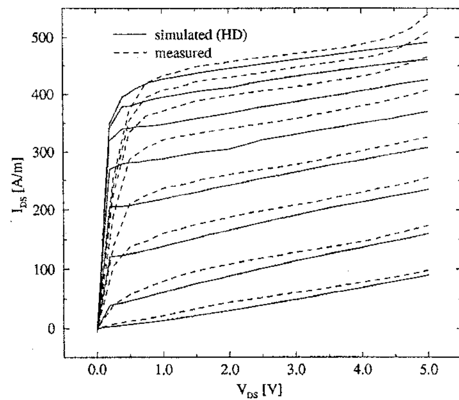

Fig. 8. Output characteristics of the low-noise HEMT

presented. HEMT are widely used in high frequency applications. Numerical simulation requires the ability to handle abrupt parameter variation across hetero-interfaces. Gate length of the simulated pseudomorphic HEMT is $L_G = 0.23\mu m$. Applied bias voltages are $V_{DS} = 5V$ and $V_{GS} = 1V$. Figure 7 shows the structure of the device and the electron temperature profile. The interface condition at the channel-to-barrier heterojunction is given by the thermionic field-emission model. A significant temperature peak can be observed at the drain-sided end of the channel. The simulated and measured output characteristics are plotted in figure 8.

VII. TCAD FRAMEWORKS

Besides the progress in physical models and computational techniques, which has dominated Technology Computer Aided Design (TCAD) in the past, aspects purely related to software technology are attracting increasing attention.

The fabrication of a modern integrated circuit may involve several hundreds of individual process steps. Virtually for each of these steps a variety of simulation tools exist. These tools are more or less peculiar about their control parameters and their representation of the wafer data. Aiming at the simulation of complete process flows the need for coupling different simulation tools in a unified manner arose. For unambiguous wafer state description the Profile Interchange Format (PIF) [73] has been proposed, and its application to couple heterogeneous tools is reported in [74]. Automatic optimization of semiconductor devices requires the repeated execution of entire simulation flows to compute a set of response variables as function of a set of control variables [75]. All these needs lead to the introduction of the framework concept in the TCAD field. The essence of this concept is to distinguish between specialized simulation tools, and the integrating framework which ties together these tools to solve actual TCAD design tasks [76][77][78].

VIII. CONCLUSION

The present situation of process modeling has been outlined. Despite the variety of process steps for each of which simulation tools have been developed the following trends can be observed: (1) modeling of three-dimensional effects is gaining importance in modern technologies; (2) the involved processes are not always understood on an atomistic level, and many parameters cannot be determined uniquely from experiments. Therefore, there is still room for model developments; (3) Automatic consecutive invocation of different process simulators is required to simulate complete process flows. Optimization of process parameters and sensitivity analysis are more complex tasks which have called for the introduction of TCAD frameworks.

Compared to the uncertainties in process modeling the mechanisms governing the electrical behavior of a device are much better understood. The widely used drift-diffusion and the hydrodynamic transport models are consistently derived from the well accepted Boltzmann equation. Basic physical parameters such as mobility and recombination rate are well accessible by experiments. However, due to the steep gradients occurring in highly miniaturized devices the accuracy of these transport models has become subject of discussion. Bigger uncertainties are observed when modeling hot carrier effects, which were not discussed in this paper, such as gate current or interface trap generation.

Process and device simulation have become an indispensable aid for the development of new semiconductor manufacturing processes. It can be foreseen that the importance of TCAD will further increase.

ACKNOWLEDGMENT

This work is supported by: Austria Mikrosysteme International – AMS at Unterpremstätten, Austria; Dig-

ital Equipment Corporation at Hudson, USA; Hitachi Ltd. at Tokyo, Japan; LSI Logic Corporation at Milpitas, USA; Motorola Inc. at Austin, USA; Philips at Eindhoven, The Netherlands; Siemens Corporation at Munich, Germany; and Sony at Atsugi, Japan.

References

[1] H. Gummel, "A Self-Consistent Iterative Scheme for One-Dimensional Steady State Transistor Calculations," *IEEE Trans.Electron Devices*, vol. ED-11, pp. 455–465, 1964.

[2] A. Wong, R. Guerrieri, and A. Neureuther, "Massively Parallel Electromagnetic Simulation for Photolithographic Applications," *IEEE Trans.Computer-Aided Design*, vol. 14, no. 10, pp. 1231–1240, 1995.

[3] K. Lucas, H. Tanabe, C. Yuan, and A. Strojwas, "Efficient and Rigorous 3D Model for Optical Lithography Simulatation," in *1995 International Conference on Simulation of Semiconductor Processes and Devices*, (Erlangen, Germany), pp. 14–17, Springer, 1995.

[4] H. Kirchauer and S. Selberherr, "Rigorous Three-Dimensional Photolitography Simulation Over Nonplanar Structures," in *ESSDERC'96 - 26th European Solid State Device Research Conference* (G. Baccarani and M. Rudan, eds.), (Gif-sur-Yvette Cedex, France), pp. 347–350, Editions Frontieres, 1996.

[5] V. Axelrad, "Fast and Accurate Areal Imaging Simulation for Layout Printability Otimization," in *1995 International Conference on Simulation of Semiconductor Processes and Devices*, (Erlangen, Germany), pp. 10–13, Springer, 1995.

[6] K. Toh, A. Neureuther, and E. Scheckler, "Algorithms for Simulation of Three-Dimensional Etching," *IEEE Trans.Computer-Aided Design*, vol. 13, no. 5, pp. 616–624, 1994.

[7] E. Scheckler, N. Tam, A. Pfau, and A. Neureuther, "An Efficient Volume-Removal Algorithm for Practical Three-Dimensional Lithography Simulation with Experimental Verification," *IEEE Trans.Computer-Aided Design*, vol. 12, pp. 1345–1356, 1993.

[8] W. Henke, D. Mewes, M. Weiß, G. Czech, and R. Schließl-Hoyler, "A Study of Reticle Defects Imaged into Three-Dimensional Developed Profiles of Positive Photoresists Using the SOLID Lithography Simulator," *Microelectr.Eng.*, vol. 14, pp. 283–297, 1991.

[9] Y. Hirai, S. Tomida, K. Ikeda, M. Sasago, M. Endo, S. Hayama, and N. Nomura, "Three-Dimensional Resist Process Simulator PEACE (Photo and Electron Beam Lithography Analyzing Computer Engineering System)," *IEEE Trans.Computer-Aided Design*, vol. 10, pp. 802–807, June 1991.

[10] T. Ishizuka, "Bulk Image Effects of Photoresist in Three-Dimensional Profile Simulation," *COMPEL*, vol. 10, pp. 389–399, 1991.

[11] A. Moniwa, T. Matsuzawa, T. Ito, and H. Sunami, "Three-Dimensional Photoresist Imaging Process Simulator for Strong Standing-Wave Effect Enviroment," *IEEE Trans.Computer-Aided Design*, vol. CAD-6, pp. 431–437, 1987.

[12] E. Scheckler and A. Neureuther, "Models and Algorithms for Three-Dimensional Topography Simulation with SAMPLE-3D," *IEEE Trans.Computer-Aided Design*, vol. 13, no. 2, pp. 219–230, 1994.

[13] J. Pelka, "Three-Dimensional Simulation of Ion-Enhanced Dry-Etch Processes," *Microelectr.Eng.*, vol. 14, pp. 269–281, 1991.

[14] S. Tazawa, F. Leon, G. Anderson, T. Abe, K. Saito, A. Yoshii, and D. Scharfetter, "3-D Topography Simulation of Via Holes Using Generalized Solid Modeling," in *Int.Electron Devices Meeting*, pp. 173–176, 1992.

[15] M. Fujinaga, N. Kotani, T. Kunikiyo, H. Oda, M. Shirahata, and Y. Akasaka, "Three-Dimensional Topography Simulation Model: Etching and Lithography," *IEEE Trans.Electron Devices*, vol. 37, pp. 2183–2192, Oct. 1990.

[16] E. Strasser and S. Selberherr, "Algorithms and Models for Cellular Based Topography Simulation," *IEEE Trans.Computer-Aided Design*, vol. 14, no. 9, pp. 1104–1114, 1995.

[17] H. Ryssel and I. Ruge, *Ion Implantation*. New York: Wiley, 1986.

[18] J. Lindhard, M. Scharff, and H. Schiøtt, "Range Concepts and Heavy Ion Ranges," *Mat.Fys.Medd.Dan.Vid.Selsk.*, vol. 33, no. 14, pp. 1–42, 1963.

[19] J. Gibbons, W. Johnson, and S. Mylroie, *Projected Range Statistics*. Strandsberg: Halstead Press, 1975.

[20] D. Antoniadis, S. Hansen, and R. Dutton, "SUPREM II – A Program for IC Process Modeling and Simulation," Tech. Rep. 5019-2, Stanford University, 1978.

[21] A. D. Keersgieter, L. Dupas, and K. D. Meyer, "Implantation and Diffusion Modelling of Boron in Silicon," in *ESSDERC'87*, pp. 423–425, 1987.

[22] R. Wilson, "Random and Channeled Implantation Profiles and Range Parameters for P and Al in Crystalline and Amorphized Si," *J.Appl.Phys.*, vol. 60, no. 8, pp. 2797–2805, 1986.

[23] A. Tasch, H. Shin, C. Park, J. Alvis, and S. Novak, "An Improved Approach to Accurately Model Shallow B and BF_2 Implants in Silicon," *J.Electrochem.Soc.*, vol. 136, no. 3, pp. 810–814, 1989.

[24] H. Ryssel, J. Lorenz, and K. Hoffmann, "Models for Implantation into Multilayer Targets," *Appl.Phys.A*, vol. 41, pp. 201–207, 1986.

[25] H. Ryssel, J. Lorenz, and W. Krüger, "Ion implantation into non-planar targets: Monte Carlo simulation and analytical methods," *Nucl.Instr. and Methods in Physics Research*, vol. B19/20, pp. 45–49, 1987.

[26] G. Hobler, E. Langer, and S. Selberherr, "Two-Dimensional Modeling of Ion Implantation with Spatial Moments," *Solid-State Electron.*, vol. 30, no. 4, pp. 445–455, 1987.

[27] M. Thompson, "An Introduction to Channeling," in *Channeling – Theory, Observation and Applications* (D. Morgan, ed.), ch. 1, pp. 1–36, New York: Wiley, 1973.

[28] G. Hobler and H. Pötzl, "Electronic Stopping of Channeled Ions in Silicon," in *Mat.Res.Soc.Symp.Proc.*, vol. 279, pp. 165–170, 1993.

[29] G. Hobler, A. Simionescu, L. Palmetshofer, C. Tian, and G. Stingeder, "Boron Channeling Implantations in Silicon: Modeling of Electronic Stopping and Damage Accumulation," *J.Appl.Phys.*, vol. 77, no. 8, pp. 3697–3703, 1995.

[30] A. Simionescu, *Monte-Carlo-Simulation der Ionenimplantation in kristallinem Silizium*. Dissertation, Technische Universität Wien, 1995.

[31] H. Stippel, *Simulation der Ionen-Implantation*. Dissertation, Technische Universität Wien, 1993.

[32] W. Bohmayr, *Simulation der Ionenimplantation in kristalline Siliziumstrukturen*. Dissertation, Technische Universität Wien, 1996.

[33] L. Christel, J. Gibbons, and S. Mylroie, "An Application of the Boltzmann Transport Equation to Ion Range and Damage Distribution in Multilayered Targets," *J.Appl.Phys.*, vol. 51, no. 12, pp. 6176–6182, 1980.

[34] M. Giles, "Ion Implantation Calculations in Two Dimensions Using the Boltzmann Transport Equation," *IEEE Trans.Computer-Aided Design*, vol. CAD-5, no. 4, pp. 679–684, 1986.

[35] P. Fahey, P. Griffin, and J. Plummer, "Point Defects and Dopant Diffusion in Silicon," *Review of Modern Physics*, vol. 61, no. 2, pp. 289–384, 1989.

[36] J. Crank, *The Mathematics of Diffusion*. Clarendon Press, second ed., 1975.

[37] K. Lehovec and A. Slobodskoy, "Diffusion of charged particles into a semiconductor under consideration of the built-in field," *Solid-State Electron.*, no. 3, p. 45, 1961.

[38] R. Shrivastava and A. Marshak, "A model for diffusion of arsenic in degenerate silicon," *J.Appl.Phys.*, vol. 51, pp. 3222–3229, 1980.

[39] S. Hu, "Diffusion in Heavily Doped Semiconductors: Local Charge Neutrality and One-Band Approximations," *J.Appl.Phys.*, vol. 43, no. 4, pp. 2015–2018, 1972.

[40] R. Fair, "Concentration Profiles of Diffused Dopants," in *Impurity Doping Processes in Silicon* (F. Wang, ed.), pp. 315–442, North-Holland, 1981.

[41] E. Guerrero, H. Pötzl, R. Tielert, M. Grasserbauer, and G. Stingeder, "Generalized Model for the Clustering of As Dopants in Si," *J.Electrochem.Soc.*, vol. 129, no. 8, pp. 1826–1831, 1982.

[42] K. Wimmer, *Two-Dimensional Nonplanar Process Simulation.* Dissertation, Technische Universität Wien, 1993.

[43] D. Antoniadis, A. Gonzales, and R. Dutton, "Boron in Near-Intrinsic ⟨100⟩ and ⟨111⟩ Silicon under Inert and Oxidizing Ambients–Diffusion and Segregation," *J.Electrochem.Soc.*, vol. 125, no. 5, pp. 813–819, 1978.

[44] M. Giles, "Defect-Coupled Diffusion at High Concentrations," *IEEE Trans.Computer-Aided Design*, vol. 8, no. 5, pp. 460–467, 1989.

[45] R. Dürr and P. Pichler, "A Consistent Pair-diffusion Based Steady-state Model for Phosphorus Diffusion," in *ESSDERC'89*, pp. 297–301, 1989.

[46] W. Richardson and B. Mulvaney, "Plateau and kink in P profiles diffused into Si: A result of strong bimolecular recombination?," *Appl.Phys.Lett.*, vol. 53, pp. 1917–1919, 1988.

[47] J. Lorenz, ed., *3-Dimensional Process Simulation*, (Wien), Springer, 1995.

[48] S. Selberherr, *Analysis and Simulation of Semiconductor Devices.* Wien: Springer, 1984.

[49] K. Blotekjaer, "Transport Equations for Electrons in Two-Valley Semiconductors," *IEEE Trans.Electron Devices*, vol. ED-17, pp. 38–47, Jan. 1970.

[50] P. Landsberg and S. Hope, "Two Formulations of Semiconductor Transport Equations," *Solid-State Electron.*, vol. 20, pp. 421–429, 1977.

[51] G. Baccarani and M. Wordeman, "An Investigation of Steady-State Velocity Overshoot in Silicon," *Solid-State Electron.*, vol. 28, no. 4, pp. 407–416, 1985.

[52] M. Rudan and F. Odeh, "Multi-Dimensional Discretization Scheme for the Hydrodynamic Model of Semiconductor Devices," *COMPEL*, vol. 5, no. 3, pp. 149–183, 1986.

[53] R. Cook and J. Frey, "An Efficient Technique for Two-Dimensional Simulation of Velocity Overshoot Effects in Si and GaAs Devices," *COMPEL*, vol. 1, no. 2, pp. 65–87, 1982.

[54] Y. Feng and A. Hintz, "Simulation of Submicrometer GaAs MESFET's Using a Full Dynamic Transport Model," *IEEE Trans.Electron Devices*, vol. 35, pp. 1419–1431, Sept. 1988.

[55] D. Chen, E. Kan, U. Ravaioli, C. Shu, and R. Dutton, "An Improved Energy Transport Model Including Nonparabolicity and Non-Maxwellian Distribution Effects," *IEEE Electron Device Lett.*, vol. 13, pp. 26–28, Jan. 1992.

[56] K. Hennacy, N. Goldsman, and I. Mayergoyz, "2-Dimensional Solution to the Boltzmann Transport Equation to Arbitrarily High-Order Accuracy," in *Proceedings of the International Workshop on Computational Electronics*, (Leeds), pp. 118–122, Aug. 1993.

[57] A. Gnudi, D. Ventura, and G. Baccarani, "Two-dimensional MOSFET Simulation by Means of a Mulitdimensional Spherical Harmonics Expansion of the Boltzmann Transport Equation," *Solid-State Electron.*, vol. 36, no. 4, pp. 575–581, 1993.

[58] M. Fischetti and S. Laux, "Monte Carlo Analysis of Electron Transport in Small Semiconductor Devices Including Band-Structure and Space-Charge Effects," *Physical Review B*, vol. 38, pp. 9721–9745, Nov. 1988.

[59] F. Venturi, R. Smith, E. Sangiorgi, M. Pinto, and B. Ricco, "A General Purpose Device Simulator Coupling Poisson and Monte Carlo Transport with Applications to Deep Submicron MOSFET's," *IEEE Trans.Computer-Aided Design*, vol. 8, pp. 360–369, Apr. 1989.

[60] H. Kosina and S. Selberherr, "A Hybrid Device Simulator that Combines Monte Carlo and Drift-Diffusion Analysis," *IEEE Trans.Computer-Aided Design*, vol. 12, no. 2, pp. 201–210, 1994.

[61] T. Simlinger, H. Brech, T. Grave, and S. Selberherr, "Simulation of Submicron Double-Heterojunction High Electron Mobility Transistor with MINIMOS-NT," *IEEE Trans.Electron Devices*, vol. 44, no. 5, pp. 700–707, 1997.

[62] M. Mock, *Analysis of Mathematical Models of Semiconductor Devices.* Dublin: Boole Press, 1983.

[63] N. Ula, G. Cooper, J. Davidson, S. Swierkowski, and C. Hunt, "Optimization of Thin-Film Resistive-Gate and Capacitive-Gate GaAs Charge-Coupled Devices," *IEEE Trans.Electron Devices*, vol. 39, no. 5, pp. 1032–1040, 1992.

[64] C. Smith and S. Chamberlain, "Theory and Design Methodology for an Optimum Single-Phase CCD," *IEEE Trans.Electron Devices*, vol. 39, no. 4, pp. 864–873, 1992.

[65] H. Peifer, B. Meinerzhagen, R. Thoma, and W. Engl, "Evaluation of Impact Ionization Modeling in the Framework of Hydrodynamic Equations," in *Int.Electron Devices Meeting*, pp. 131–134, 1991.

[66] W. Quade, E. Schöll, and M. Rudan, "Impact Ionization within the Hydrodynamic Apprach to Semiconductor Transport," *Solid-State Electron.*, vol. 36, no. 10, pp. 1493–1505, 1993.

[67] A. Forghieri, R. Guerrieri, P. Ciampolini, A. Gnudi, M. Rudan, and G. Baccarani, "A New Discretization Strategy of the Semiconductor Equations Comprising Momentum and Energy Balance," *IEEE Trans.Computer-Aided Design*, vol. 7, pp. 231–242, Feb. 1988.

[68] T. Tang, "Extension of the Scharfetter-Gummel Algorithm to the Energy Balance Equation," *IEEE Trans.Electron Devices*, vol. ED-31, pp. 1912–1914, Dec. 1984.

[69] W.-S. Choi, J.-G. Ahn, Y.-J. Park, H.-S. Min, and C.-G. Hwang, "A Time Dependent Hydrodynamic Device Simulator SNU-2D With New Discretization Scheme and Algorithm," *IEEE Trans.Computer-Aided Design*, vol. 13, no. 7, pp. 899–908, 1994.

[70] C. Fischer, *Bauelementsimulation in einer computergestützten Entwurfsumgebung.* Dissertation, Technische Universität Wien, 1994.

[71] W. Hänsch, M. Orlowski, and W. Weber, "The Hot-Electron Problem in Submicron MOSFET," in *18th European Solid State Device Research Conference - ESSDERC 88* (J.-P. Nougier and D. Gasquet, eds.), vol. 49 of *Journal de Physique*, (Les Ulis Cedex, France), pp. 597–606, les éditions de physique, 1988.

[72] C. Köpf, H. Kosina, and S. Selberherr, "Mobility model for III-V compounds suited for hydrodynamic device simulation," in *Compound Semiconductors 1995*, no. 145 in Institute of Physics Conference, (Cheju Island, Korea), pp. 1255–1260, 22nd Int. Symp. on Compound Semiconductors, IOP Publishing Ltd, 1995.

[73] S. Duvall, "An Interchange Format for Process and Device Simulation," *IEEE Trans.Computer-Aided Design*, vol. 7, no. 7, pp. 741–754, 1988.

[74] F. Fasching, W. Tuppa, and S. Selberherr, "VISTA-The Data Level," *IEEE Trans.Computer-Aided Design*, vol. 13, no. 1, pp. 72–81, 1994.

[75] C. Pichler, N. Khalil, G. Schrom, and S. Selberherr, "TCAD Optimization Based on Task-Level Framework Services," in *Simulation of Semiconductor Devices and Processes* (H. Ryssel and P. Pichler, eds.), vol. 6, (Wien), pp. 70–73, Springer, 1995.

[76] S. Halama, F. Fasching, C. Fischer, H. Kosina, E. Leitner, P. Lindorfer, C. Pichler, H. Pimingstorfer, H. Puchner, G. Rieger, G. Schrom, T. Simlinger, M. Stiftinger, H. Stippel, E. Strasser, W. Tuppa, K. Wimmer, and S. Selberherr, "The Viennese Integrated System for Technology CAD Applications," *Microelectronics Journal*, vol. 26, no. 2/3, pp. 137–158, 1995.

[77] S. Halama, C. Pichler, G. Rieger, G. Schrom, T. Simlinger, and S. Selberherr, "VISTA—User Interface, Task Level, and Tool Integration," *IEEE Trans.Computer-Aided Design*, vol. 14, no. 10, pp. 1208–1222, 1995.

[78] F. Fasching, S. Halama, and S. Selberherr, eds., *Technology CAD Systems*, (Wien), Springer, 1993.